Contrasting early Holocene temperature variations between monsoonal East Asia and westerly dominated Central Asia

Jiaju Zhao[a], Chen-Bang An[a, *], Yongsong Huang[b, d, *], Carrie Morrill[c], Fa-Hu Chen[a]

[a] *Key Laboratory of Western China's Environmental Systems, College of Earth and Environmental Sciences, Lanzhou University, Lanzhou 730000, China*

[b] *Department of Earth, Environmental and Planetary Sciences, Brown University, Providence, RI 02912, United States*

[c] *Cooperative Institute for Research in Environmental Sciences, University of Colorado and NOAA National Climatic Data Center, Boulder, CO 80305, USA*

[d] *Institute of Earth Environment, Chinese Academy of Sciences, Xi'an, 710061, China*

* Corresponding authors.

E-mail address: cban@lzu.edu.cn; Yongsong_Huang@brown.edu

ABSTRACT

Numerous studies have demonstrated that there are major differences in the timing of maximum Holocene precipitation between the monsoonal East Asia and westerly dominated Central Asia, but it is unclear if the moisture differences are also associated with corresponding temperature contrasts. Here we present the first alkenone-based paleotemperature reconstructions for the past 21 kyr from Lake Balikun, central Asia. We show, unlike the initiation of Holocene warm conditions at ~11 kyr BP in the monsoon regions, the arid central Asia remained in a glacial-like cold condition prior to 8 kyr BP and experienced abrupt warming of ~9 °C after the collapse of the Laurentide ice sheet. Comparison with pollen and other geochemical data indicates the abrupt warming is closely associated with major increase in the moisture supply to the region. Together, our multiproxy data indicate ~2 thousand years delay of temperature and moisture optimum relative to local summer insolation maximum, suggesting major influence of the Laurentide ice sheet and other high latitude ice sheet forcings on the regional atmospheric circulation. In addition, our data reveal a temperature drop by ~ 4 °C around 4 kyr BP lasting multiple centuries, coinciding with severe increases in aridity previously reported based on multiproxy data. In contrast, model simulations display a much less pronounced delay in the initiation of Holocene warm conditions, raising unresolved questions about the relative importance of local radiative forcing and high-latitude ice on temperature in this region.

Keywords: Paleotemperature reconstructions; Alkenone; Central Asia; Lake Balikun

1. Introduction

There have been extensive studies of moisture changes in China and central Asia from LGM to present (e.g., Dykoski et al., 2005; Herzschuh, 2006; Chen et al., 2008; An et al., 2012, 2013; Z. An et al., 2012; Wang and Feng et al., 2013). Broadly speaking, there are two moisture source regimes: southeastern China is dominated by summer monsoon precipitation originating from the tropical Pacific and Indian Oceans, whereas central Asia and northwestern China are dominated by moisture from the Westerlies (Zhou et al., 2009; Liu et al., 2014; Chen et al., 2008). A large amount of paleohydrological data indicate overall drier conditions during the glacial and wetter conditions during the Holocene for both regimes, with the exception of a distinct difference for the timing of Holocene Climate Optimum: the Central Asia region during the middle Holocene 8 - 6 kyr BP (e.g., An et al., 2012; Chen et al., 2008), but the summer monsoon region around 11.5 - 5 kyr BP (e.g., Z. An et al., 2012; Dykoski et al., 2005). Such difference has been attributed to the influence of the last substantial remnants of northern Hemisphere ice-sheets on the atmospheric circulation (Chen et al., 2008), including the Laurentide ice sheet (LIS) and the Fennoscandian ice sheet (FIS) (Linden et al., 2006; Carlson et al., 2008). Alternatively, some model simulations of the early Holocene indicate that ice sheets had little effect on central Asian aridity, instead decreased winter temperatures over the North Atlantic due to early Holocene orbital forcing had a significant impact on evaporation and atmospheric moisture (Jin et al. 2012).

In contrast to hydrological history, our knowledge of temperature variations for the region is much less complete. Pollen data provide a long term estimate of temperature changes for relatively wet regions in southeastern China (e.g., Zhu et al., 2008). Geochemical data from Chinese loess plateau (Peterse et al., 2011; Gao et al., 2012; Jia et al., 2013) and Lake Qinghai (Hou et al., 2016) provide higher resolution reconstructions of temperature changes for the summer monsoon regions. The overall pattern is that the regional temperature responds strongly to summer insolation changes (Gao et al., 2012; Hou et al., 2016), but with major interruption at times of reduced North Atlantic Deepwater (NADW) formation, as well as around 8.2 kyr BP (Hou et al., 2016).

However, temperature variations are poorly known for the westerly-dominated central Asia. Regional vegetation is primarily controlled by moisture hence reconstruction of temperature based on pollen induces major uncertainties. Thus, a major scientific question is whether the observed difference in delayed timing of hydrological change during the early Holocene in central Asia can also be found in the temperature record. In modern conditions, cold conditions are generally associated with dry conditions, and therefore, we hypothesize that temperature in the early Holocene may also exhibit delayed warming, coeval with moisture variations.

Here we present a high-resolution alkenone-based paleotemperature reconstruction from Lake Balikun, in central Asia. The central objective is to test the hypothesis that the delayed moisture optimum during the Holocene at Lake Balikun is also associated with delayed temperature optimum in central Asia.

2. Material and methods

2.1. Study area

Lake Balikun (43.60-43.73°N, 92.74-92.84°E, 1570 m a. s. l.) is a closed-basin, hyper-saline lake (salinity 93.8 to 126.4 g/L), situated in the eastern Tianshan Mountains, western China (Fig. 1; Fig. S1) (Zhao et al., 2014; Zhao et al., 2015). Previous study suggested that the Lake Balikun was always a closed basin during the late Quaternary (Ma et al., 2004). The Lake Balikun has an area of 116.0 km^2 within a catchment of approximately 4500 km^2, sandwiched by Balikun Mountains in the south and Moqinwula Mountains in the northeast (Wang and Dou, 1998) (Fig. S1). The prominent mountain peaks in the catchment area have elevations of approximately 3800 to 4319 m a.s.l. (Fig. S1). The annual precipitation near Lake Balikun ranges from to 120 to 342 mm, with 54 ± 9 (1σ) % falling in the summer months (June to August), based instrumental data from 1960 to 2008 (Zhao et al., 2015). The lake water is supplied by Dahe River, which originates on the northern slopes of the Balikun Mountains, runs along the steppe from east to west and finally discharges into the Lake Balikun (Fig. S1). Dahe River water derives from both summer rain and spring-melting of snow accumulated during the winter and early spring on Balikun Mountains: the percentage of water from these two sources depends on seasonal distribution of rainfall. Lake Balikun reaches maximum surface area either during the summer at the peak rainy season, or during spring following the major melt water discharge, again depending on shifts in seasonal precipitation patterns. The prevailing wind directions in all seasons are west to east or northwest to southeast (summer monsoon thus does not reach this region). In recent years, permanent glaciers on surrounding mountains have disappeared, hence no longer provide sustained water supply to Dahe River during the warm seasons. The mean annual temperature in the drainage basin is ~1.9 °C (monthly minimum -24.6 °C, maximum 21.3 °C). A cool and dry season occurs in this region during the boreal winter when the Siberian High establishes, giving rise to a strong anticyclone over Eurasia inland; conversely, a relatively warm and wet season prevails during the summer months when the Siberian High diminishes and the Westerlies climate dominates (Fig. S2). Thus, Lake Balikun is an ideal site to study the variability of Westerlies and climate change in the arid central Asia.

2.2. Sediment core and dating

A 62.53 m sediment core (BLK11A: 43°39′51.05″N, 92°48′10.12″E) was retrieved from the center of Lake Balikun in June 2011 using a Kullenberg Uwitech Coring System (Zhao et al., 2015). It was sampled continuously every 1 cm for the core. In this paper, we focus on the top 6.42 m of the core. Here, we measured two accelerator mass spectrometry (AMS) ^{14}C dates measured by Beta Analytic Inc, USA on bulk sediment, together with our published ^{14}C ages (Zhao et al., 2015), are used to generate the chronology of the top 6.42 m core.

2.3. Water filters samples collection

The water filters have been widely used to explore the relationship between long chain alkenones (LCAs) and temperature when it is unclear what the alkenone-producing species in the study area is, and thus, culture experiments cannot be performed (Goni et al., 2004; Mercer et al., 2005; Toney et al., 2010; D’Andrea et al., 2011; Wang and Liu, 2013; Longo et al., 2016). To determine the relationship between summer temperatures and alkenone unsaturation, we sampled water column samples from Lake Balikun in June, July and August, but found alkenones only in June and July samples (Table S1). 24 surface water filters were collected from Lake Balikun and 8 surface water filter samples from a small unnamed lake (43.82°N, 95.04 °E, 400 m a. s. l.) 170 km northeast of Lake Balikun are collected and also used for calibrating alkenone temperature relationship (Table S1). It is a closed basin lake with a salinity 30 g/L, area of 1 km^2, and maximum depth of 1 m. Ten to twenty liters of water were filtered with combusted (550 °C) Whatman GF/F 0.7 μm, 47mm glass filters. During this time, water temperatures range from 17.6 to 27.1 °C in Lake Balikun and from 25.1 to 30.2 °C in another lake.

2.4. LOI analysis

The sediment core was sub-sampled by a 1 cm interval for loss-on-ignition analysis. Sequential combustion at 550 °C and 950 °C was used to estimate organic matter (Loss-on-ignition; LOI) and carbonate contents, respectively (modified from Dean, 1974).

2.5. Alkenone analysis

A total of 120 sediment samples from BLK11A core and 32 water filters were analyzed for LCAs at Brown University using the method described previously (Zhao et al., 2014). All except for 16 samples in BLK11A contain sufficient alkenones for quantification. Briefly, sediment samples (1-7 g) and water filters were freeze-dried and then extracted with dichloromethane (DCM) via an Accelerated Solvent Extractor ASE200 (Dionex). The extract was separated into neutral and acid fractions on a LC-NH_2 SPE column. The neutral fraction was separated into the aliphatic (n-hexane), ketone (DCM) and polar (Methanol) fractions using silica gel column chromatography. The ketone fractions were then saponified and further cleaned up using silica gel columns. The alkenone fractions were analyzed using an Agilent 6890plus Gas Chromatograph equipped with a VF-200ms GC column and a Flame Ionization Detector (FID) for quantification (Longo et al., 2013). Alkenones were identified by comparison of retention time with alkenone standards as well as confirmation using GCMS analyses (Longo et al., 2013; Zhao et al., 2014). LCA concentrations were determined on GC-FID using the C_{36} *n*-alkane standard.

3. Results

3.1. Lithology and chronology

We have published the pollen and grain-size data during MIS2 and last deglaciation (294-720) in the BLK11A core (Zhao et al., 2015). In this paper, we focus on the top 6.42 m of the core, which is consisted of clay (5.7–6.42 m), black clay (5.4–5.7 m), silt with sand (4.8-5.4 m), dark clay (3.4-4.8 m), black clay (2.9-3.4 m), clay (1.6-2.9 m) with a few Mirabilite crystals ($Na_2SO_4 \cdot 10H_2O$) and Mirabilite crystals (1.6-0 m). Ten AMS ^{14}C ages were used to generate an independent chronology (Table 1). After correcting for the 790 years reservoir and converting corrected radiocarbon ages to calendar ages by Calib 7.0 software (An et al., 2012; Reimer et al., 2013; Zhao et al., 2015), ages of each sampling interval are established by linear interpolation between the two adjoining calendar year ages (Fig. 2).

3.2. U_{37}^{k}-temperature calibration based on modern water filters samples

32 surface water samples were analyzed for LCAs which were absent in 2 samples (Table S1). C_{37}-C_{40} LCAs were detected in surface water samples, but C_{39}-C_{40} LCAs were absent in most samples. The relative abundance of C_{37} alkenones relative to C_{38} alkenones, expressed as $C_{37}/C_{38} = (C_{37:4} + C_{37:3} + C_{37:2})/ (C_{38:4} + C_{38:3} + C_{38:2})$. The C_{37}/C_{38} ratios range from 0.4 to 1.2, and the average value is 0.69 in surface water samples. The U_{37}^{k} index [$U_{37}^{k} = (C_{37:2} - C_{37:4})/ (C_{37:4} + C_{37:3} + C_{37:2})$] has a significant relationship to lake water temperature (y = 0.015x -0.678, $r^2 = 0.66$, $p<0.01$) (Fig. 3a); whereas the $U_{37}^{k\prime}$ index [$U_{37}^{k\prime} = C_{37:2}/ (C_{37:3} + C_{37:2})$] shows no correlation to lake water temperature (Fig. 3b). The same phenomenon was reported in the *in-situ* work from Lake George (Toney et al., 2010), and culture experiments (Theroux et al., 2010; Nakamura et al., 2014). We also measured the in-situ air temperature, and found a strong relationship between *in-situ* air temperature and *in-situ* water temperature (Fig. S3). Therefore, we suggest that surface lake water temperature reflects air temperature in Lake Balikun.

3.3. LOI values

Organic matter content as assessed by LOI ranges from 2.7 to 20 % and displays large variations throughout the sediment core (Fig. 4). LOI varied around a mean value of ~ 6.9 ± 1.8 % between 21 and 17 kyr BP, but decrease significantly to a mean value of 5.9 ± 1.7 % (min 2.7 %, max 12.1 %) between 17 and 9.3 kyr BP. LOI began to rise after 9.5 kyr BP, and oscillated around 8.2 kyr BP. The highest LOI values were reached during the mid-Holocene (~8 - 6 kyr BP), followed by a continuously decreasing trend after 6 kyr BP.

From 21 to 9.3 kyr BP, the carbonate content was generally lower than 10 % except two periods around 20-17 kyr BP and 14.9-12.8 kyr BP. After 9.3 kyr, the carbonate content began to increase and reach maximum (85%) around 8 kyr BP, following a decreasing trend after 8 kyr BP.

3.4. Paleotemperature reconstructions based on alkenones

The total LCA concentrations (C_{37} - C_{40}) were relatively low during the glacial and early Holocene before ~8.2 kyr BP, around 0.4 to 2.6 μg/g of dry sediment and occasionally absent. Immediately after 8.2 kyr BP, the LCA concentrations increased abruptly, ranging from 2.6 to 192 μg/g of dry sediment (Fig. 4). GC-MS showed that odd and even carbon number alkenones were methyl and ethyl ketones, respectively. In majority of the samples, alkenones are characterized by the presence of C_{40} LCAs but lack C_{38} methyl and C_{39} ethyl alkenones, indicate the presence alkenone producers closely related to coastal haptophyte species (*Chrysotilla lamellosa*, *Isochrysis galbana* and *Pseudoisochrysis paradoxa*) (Theroux et al., 2010).

Previous studies suggest that there are two major types of haptophytes in saline lakes (Theroux et al., 2010; Toney et al., 2012; D'Andrea, et al., 2016). Key differences between the two species are the relative abundance of C_{37}/C_{38} alkenones and $\%C_{37:4}$ alkenone (Chu et al., 2005; Pearson et al., 2008; Toney et al., 2010; Wang et al., 2015). Different species of haptophytes could dominate during different periods in the past (Coolen et al., 2004; Randlett et al., 2014) due to lacustrine environment change (e.g., salinity, nutrients). When multiple species are present in the same samples, it is generally difficult to obtain quantitative paleotemperature reconstructions and only qualitative temperature estimates could be made (e.g., Randlett et al., 2014). Fortunately, however, in the case of Lake Balikun downcore samples, we found two distinct types of alkenone profiles that appear to display little overlap (Fig. 5 and 6). One pattern (Type I) is similar to surface water samples in Lake Balikun, and it's characterized by C_{38} component dominant and high %$C_{37:4}$ (Fig. 5). In contract, another pattern (Type II) is characterized by low %$C_{37:4}$ and a large range of C_{37}/C_{38} ratio (Fig. 6). We were able to use principal component analysis (PCA) to cleanly separate the LCAs samples into two distinct clusters (Fig. 7; Fig. S4). We note that the alkenone-inferred haptophyte species changes in downcore samples are strongly correlated in timing with lake environmental change inferred pollen, LOI and carbonate content variations (Fig. 4 and Fig. S5). Type I alkenone species dominated in present, mid- and late-Holocene when the lake was stable and climate was relatively wet. In contrast, type II alkenone species dominated during around 4.2 kyr, early Holocene and glacial when the lake was small and climate was dry (Fig. S5).

To account for the species effect on reconstructed temperatures, we used different calibrations to calculate the downcore temperatures for periods when Type I and Type II alkenones are predominant (Fig. S5). Type I LCAs was similar to surface water samples in Lake Balikun, and hence we used our U_{37}^{k}-temperature calibration based on water filter samples ($T = 44.598 \times U_{37}^{k} + 38.056$, $r^2 = 0.66$, $p<0.01$, standard error = 2.12 °C, n=27) to calculate temperature (Fig. S5). The producer of type II LCAs was similar to coastal and saline lake haptophyte species (belonging to the group II) based on LCAs distribution (Fig. 6; Theroux et al., 2010). There are several published U_{37}^{k}-temperature calibrations for type II haptophytes (Sun et al., 2007; Toney et al., 2010; Theroux et al., 2013; Nakamura et al., 2014; Hou et al., 2016; Zheng et al., 2016) (Table S2). The calculated temperatures using different calibrations display the same trends but with significant offsets in absolute values: several calibrations lead to unrealistically large temperature changes around 8.2 kyr BP. For this reason, we opted to use CCMP1307 U_{37}^{k}-temperature calibration (Nakamura et al., 2014) to calculate the temperature for type II LCAs which give the temperature change at 8.2 kyr BP similar in scale to the amplitude recently reported from Mt Altai ice core (Aizen et al., 2016) (Fig. S5). At present LCAs producer is blooming mainly in June-July, hence we interpret alkenone inferred temperatures as early summer temperatures.

4. Discussions

4.1. Changes in the regional moisture history inferred from records of BLK11A core

Many previous studies have used a variety of sedimentary proxies to infer regional moisture history (Chen et al., 2008, 2016; An et al., 2012, 2013; Wang and Feng et al., 2013). Our data from BLK11A are consistent with previous conclusions. Lake Balikun is calcium limited (Zheng et al., 1995), similar to Lake Qinghai (Z. An et al., 2012), and hence higher calcium carbonate in sediments is interpreted to reflect wetter conditions and higher lake level. Carbonate data show a major peak about 8 kyr BP, suggesting major increase in precipitation possibly related to the collapse of the LIS. In lake sediments, the organic matter reflects autochthonous production from plants and input of eroded organic material from the catchment. Thus the organic content in lake sediments can be broadly corresponding with net primary production in the catchment. In the arid study site, higher organic matter in sediments is interpreted to reflect wetter conditions (Xue and Zhong, 2011). LOI data from BLK11A indicate dry conditions during the glacial and around 4 kyr BP, and peak moisture around 8 to 6 kyr BP. Although alkenone concentrations do not always follow the LOI, the major rise in alkenones after 8.2 kyr suggests aquatic productivity increased dramatically around the time. Moisture history inferred from productivity and carbonate contents are strongly supported by pollen inferred vegetation changes (An et al., 2012, 2013) (Fig. 4).

4.2. Impact of Northern Hemisphere ice sheets on regional temperature and moisture between 21 and 11.7 kyr BP

From 21 to 14.9 kyr, the average summer temperature was approximately 17.5 °C. LOI and carbonate content reflect low net primary production in the catchment and small lake area in the last glacial (Fig. 4), corresponding to the sparse desert/desert steppe vegetation documented by pollen records (An et al., 2013). Overall, multiproxy records indicate dry and cold climate conditions from the last glacial maximum to 14.9 kyr BP. The climate conditions lead to greatly expanded desert region and reduced vegetation coverage. Global climate modeling has demonstrated that ice sheet growth during the LGM led to an increase in the meridional (latitudinal) temperature gradient and southward migration of the polar front and the Westerlies (COHMAP Members., 1988; Kutzbach and Webb, 1993). The presence of permanent northern Hemisphere ice sheets (e.g., LIS and FIS) could have provided a year-round reservoir of cold air at high latitude regions, obstructing northward migration of the Westerlies while enhancing the intensity and extending the duration of Siberian High. These atmospheric circulation patterns resulted in a cold-dry climate during the LGM in central Asia.

Temperature increased by ~ 4.8 °C and was variable between 14.9 to 12.5 kyr BP, corresponding to the Bølling-Allerød period (Grootes et al., 1993; Shakun et al., 2012) (Fig. 8). During the Bølling-Allerød period, accelerated melting of mountain glaciers under warm climate condition increases the rivers runoff and the inflow of the lake, leading to the high *Artemisia*% and carbonate content (Zhao et al., 2015).

Alkenone-inferred temperatures are low during Heinrich Event 1 (H1) and the Younger Dryas (YD), but do not display the large and abrupt decreases as observed in Greenland and circum-Atlantic regions (Fig. 9). Freshwater forcing reduction of the AMOC is commonly invoked to explain millennial-scale decrease in temperatures on the Greenland ice sheet and surrounding regions (Clark et al., 2001). Our results suggest impact of changes in AMOC on the summer temperatures of our study region is limited relative to other forcings.

4.3. The delayed Holocene thermal maximum in central Asia

Summer temperature from Lake Balikun remained low prior to 8 kyr BP and experienced abrupt warming of 9 ^{o}C after the collapse of the LIS (~ 8 kyr BP), around 2 thousand years delay relative to local summer insolation (Laskar et al., 2004) (Fig. 9).

The peak summer temperature at Lake Balikun at ~ 8 kyr BP is followed by a general decline trend toward present (Fig. 8). Pollen and other geochemical data indicate the abrupt warming around 8.2 kyr BP is closely associated with major increase in the moisture supply to the region (Chen et al., 2008; An et al., 2012).

The Holocene temperature optimum from alkenones in Lake Balikun is corroborated by reconstructed moisture based on pollen and other geochemical data from lakes in the arid central Asia (e.g., Chen et al., 2008; An et al., 2012), indicating that the post glacial increase in both temperature and moisture in the region is delayed by approximately 2 kyr relative to local summer insolation maximum, while the Asian monsoon region's moisture (precipitation) generally follows summer insolation. For example, oxygen-isotope ($\delta^{18}O$) data from Dongge speleothems suggest a strong Asian summer monsoon during the early and mid-Holocene in Asian monsoon region when summer insolation is at a maximum (Dykoski et al., 2005). The summer temperature record (Hou et al., 2016) and summer monsoon index (SMI) (Z. An et al., 2012) at Lake Qinghai indicated that the Holocene Climate Optimum occurred between 11.5 and 5 kyr BP. Pollen-based annual precipitation reconstructed from Gonghai Lake gradually increased from 14.7-7.8 kyr BP, reached the highest from 7.8-5.3 kyr BP (Chen et al., 2015). In addition, in the nearby Lake Daihai, maximum precipitation also occurred during the middle Holocene (Xiao et al., 2004).

We suggest that the delayed Holocene Climate Optimum in central Asia can be attributed to the influence of the last substantial remnant northern Hemisphere ice-sheets, including the Laurentide ice sheet and the Fennoscandian ice sheet, on the atmospheric circulation as well as in the glacial periods. These post-glacial ice sheets persisted in the early Holocene (Linden et al., 2006; Carlson et al., 2008). The presence of the Northern Hemisphere ice-sheets appears to have played a key role in determining the climate in Central Asia, resulting in cold/cool and dry climate from the LGM to early Holocene. Extent of regional glaciers must also play a role on the temperatures. Studies of glacier history in the eastern Tianshan region (Zhao et al., 2012; Chen et al., 2015), where Lake Balikun is situated, suggest that there were two major periods of glacier advances since the last glacial maximum. The first period is around 15.8 ± 1.6 kyr BP and the second is during the Little Ice Age (0.79 ± 0.59 kyr BP) (Zhao et al., 2012; Chen et al., 2015). Unfortunately, the extent of the glacier during the most of the Holocene is uncertain because the major glacier advance during the Little Ice Age erased earlier evidence of glacial margin (Zhao et al., 2012; Chen et al., 2015).

In contrast, model simulations generally suggest that local insolation is most important for determining early Holocene summer temperature in Central Asia. In the CCSM3 TraCE transient simulation, for example, summer temperatures in Central Asia increase about 7 °C during the deglaciation followed by maximum temperatures between 11.7 and 8 kyr BP for June and July and around 7.8 kyr BP for August (Fig. 8). These timings for temperature maxima closely track local insolation maxima of approximately 11 kyr BP, 10 kyr BP, and 8 kyr BP for June, July, and August, respectively. Likewise, transient experiments completed with ECBilt-CLIO-VECODE show a dominant role for insolation in determining the timing of peak July warming in Eurasia south of 45-50°N (Renssen et al., 2009, 2012). Lastly, a series of time slice experiments completed with the CCSM3, designed to explore the effects of orbital and ice sheet forcings individually, indicate that both the remnant ice sheet itself and freshwater forcing from the melting of the ice sheet had a minimal effect on early Holocene summer temperatures in central Asia (Jin et al., 2012).

Several possible explanations exist for the model-data discrepancy in early Holocene summer temperature in central Asia. First, it is possible that the alkenone temperature records a later summer (e.g., August) signal, with a maximum around 8 kyr BP due to the timing of orbital forcing. Additionally, the temperature reconstruction could be impacted by the changing dominance of alkenone species and the necessity of applying different calibrations to the record. Alternatively, it is possible that the models are biased and do not show the appropriate sensitivity to orbital and ice sheet forcing for this region.

Despite differences in Holocene summer temperature trends, models and data show some agreement regarding early Holocene moisture conditions. In the TraCE experiment, the modeled rainfall is relatively low during early Holocene and increases ca. 27 mm

(16%) around 8.2 kyr BP (Liu et al., 2009) (Fig. 8). Additional work with the CCSM3 proposes that dry conditions in the early Holocene in central Asia were due to decreased temperatures and evaporation over the North Atlantic, leading to decreased water vapor advection over Eurasia (Jin et al., 2012). Thus, while both modern conditions and the alkenone record show an association between cold and dry conditions, the models simulate warm and dry conditions for the early Holocene.

4.4 The 4 kyr cold-dry event

Alkenone data indicate major summer cooling by ~4 ^{o}C between 4.8 and 3.8 kyr BP in Lake Balikun (Figs. 3 and 4). Similar amplitude scale of temperature drop is also observed in the high resolution alkenone record from Lake Qinghai (Hou et al., 2016), indicating the 4 kyr cooling event had a broader regional impact than the early Holocene climate pattern. Our alkenone data are corroborated by numerous published paleolimnological records suggesting major drought around 4 kyr BP in central Asia and monsoon region, such as Lake Daihai, Lake Hulun and Lake Tuolekule (Xiao et al., 2004; Wen et al., 2010; An et al., 2011).

Abnormal conditions in North Atlantic regions are the likely triggers for the 4 kyr cold-dry climate event in central Asia. There are a number of related events in the Atlantic including enhanced ice-rafted debris (Bond et al., 2001), weakening of AMOC (McManus et al., 2004) and a reduction Atlantic inflow between 4.8 and 3.5 kyr BP (Eldevik et al., 2014). These ocean circulation changes correspond to a major increase in the sea ice cover in the Barents Sea between 4.8 and 3.5 kyr BP (de Vernal et al., 2013), that could reflect changes in atmospheric pressure distribution and atmospheric flow which can subsequently affect regional temperature at Balikun. Not surprisingly, this event does not appear in transient model simulations (Fig. 8), which lack forcings other than orbital and greenhouse gas changes during this time period as well as a series of ensemble experiments that would be necessary to capture the wider range of variability that is capable of being generated internally within the climate system.

The distinct cold-dry climate event around 4 kyr may have exerted major influence on the prehistoric cultural exchange in Asia (Cullen et al. 2000; Staubwasser et al. 2003;

Weiss and Bradley 2001; Weiss et al. 1993; Wu and Liu 2004). The cold-dry climate event terminated many Chinese Neolithic cultures in parts of northern China, and many agricultural cultures were replaced by pastoralism or by agro-pastoralism (Liu and Feng, 2012). In the Tibetan Plateau, the cold-dry climate event likely delayed permanent human settlements on the high altitude regions (>3000 m) of the Tibetan Plateau by at least 500 years (Hou et al., 2016).

5. Conclusions

We report the first temperature reconstruction for the past 21 kyr in central Asia based on alkenones in Lake Balikun sediments. Together with multiproxy reconstructions, our results indicate a ~ 2 thousand year delay in the Holocene temperature optimum (with a temperature offset of approximately 9 °C around 8.2 kyr BP relative to the local summer insolation maximum in central Asia, in consistent with the temporal change in the the numerous published reconstructions of moisture variations. We attribute such delay in temperature and precipitation optimum during the early Holocene to the major influence of northern Hemisphere high latitude ice sheets forcings on the regional atmospheric circulation. In addition, our data indicate a major decrease in temperature by ~ 4 ^{o}C around 4 kyr BP lasting multiple centuries, coinciding with severe increases in aridity previously reported based on multiproxy data. Comparison with sea ice cover in the Barents Sea suggests cooling of the moisture regions for the westerlies might have driven this abrupt change in temperature and moisture around 4 kyr BP. Model simulations display a much less pronounced delay in the early Holocene temperature optimum and instead tend to track insolation, raising important questions about the relative sensitivity of this region to local radiative forcing compared to high-latitude ice sheets.

Acknowledgments

This work was supported by the National Natural Science Foundation of China (Grant No. 41671189, 41372180) and the National Science Foundation (Grant No. ATM-0902805). We are grateful to two anonymous reviewers for their thoughtful reviews that helped to significantly improve this manuscript.

References

Aizen, E.M., Aizen, V.B., Takeuchi, N., Mayewski, P.A., Grigholm, B., Joswiak, D.R., Nikitin, S.A., Fujita, K., Nakawo, M., Zapf, A., 2016. Abrupt and moderate climate changes in the mid-latitudes of Asia during the Holocene. J. Glaciol. 62 (233) 411–439.

An, C.B., Lu, Y., Zhao, J., Tao, S., Dong, W., Li, H., Jin, M., Wang, Z., 2012. A high-resolution record of Holocene environmental and climatic changes from Lake Balikun (Xinjiang, China): Implications for central Asia. Holocene, 22, 43-52.

An, C.B., Tao, S.-C., Zhao, J., Chen, F.-H., Lv, Y., Dong, W., Li, H., Zhao, Y., Jin, M., Wang, Z., 2013. Late Quaternary (30.7–9.0 cal ka BP) vegetation history in Central Asia inferred from pollen records of Lake Balikun, northwest China. J. Paleolimnol. 49, 145-154.

An, C.B., Zhao, J., Tao, S., Lv, Y., Dong, W., Li, H., Jin, M., Wang, Z., 2011. Dust variation recorded by lacustrine sediments from arid Central Asia since ~ 15 cal ka BP and its implication for atmospheric circulation. Quat. Res. 75, 566-573.

An, Z., Colman, S. M., Zhou, W., Li, X., Brown, E.T., Jull, A. J.T., Cai, Y., Huang, Y., Lu, X., Chang, H., Song, Y., Sun, Y., Xu, H., Liu, W., Jin, Z., Liu, X., Cheng, P., Liu, Y., Ai, L., Li, X., Liu, X., Yan, L., Shi, Z., Wang, X., Wu, F., Qiang, X., Dong, J., Lu, F., Xu, X., 2012.Interplay between the Westerlies and Asian monsoon recorded in Lake Qinghai sediments since 32 ka: Sci. Rep. 2, 619.

Bond, G., Kromer, B., Beer, J., Muscheler, R., Evans, M.N., Showers, W., Hoffmann, S., Lotti-Bond, R., Hajdas, I., Bonani, G., 2001. Persistent Solar Influence on North Atlantic Climate During the Holocene. Science 294, 2130-2136.

Bond, G., Showers, W., Cheseby, M., Lotti, R., Almasi, P., deMenocal, P., Priore, P., Cullen, H., Hajdas, I., Bonani, G., 1997. A Pervasive Millennial-Scale Cycle in North Atlantic Holocene and Glacial Climates. Science 278, 1257-1266.

Carlson, A.E., LeGrande, A.N., Oppo, D. W., Came, R.E., Schmidt, G.A., Anslow, F.S., Licciardi, J.M., Obbink, E.A., 2008. Rapid early Holocene deglaciation of the Laurentide ice sheet. Nature Geosci. 1, 620-624.

Chen, F., Xu, Q., Chen, J., Birks, H. J.B., Liu, J., Zhang, S., Jin, L., An, C., Telford, R.J., Cao, X., Wang, Z., Zhang, X., Selvaraj, K., Lu, H., Li, Y., Zheng, Z., Wang, H., Zhou, A., Dong, G., Zhang, J., Huang, X., Bloemendal, J., Rao, Z., 2015. East Asian summer monsoon precipitation variability since the last deglaciation. Sci. Rep. 5, 11186.

Chen, F., Yu, Z., Yang, M., Ito, E., Wang, S., Madsen, D.B., Huang, X., Zhao, Y., Sato, T., John B. Birks, H., Boomer, I., Chen, J., An, C., Wünnemann, B., 2008. Holocene moisture evolution in arid central Asia and its out-of-phase relationship with Asian monsoon history. Quat. Sci. Rev. 27, 351-364.

Chen Y., Li Y., Wang Y., Zhang M., Cui Z., Yi C., Liu G., 2015. Late Quaternary glacial history of the Karlik Range, easternmost Tian Shan, derived from 10Be surface exposure and optically stimulated luminescence datings. Quat. Sci. Rev.115, 17-27.

Chu, G., Sun, Q., Li, S., Zheng, M., Jia, X., Lu, C., Liu, J., Liu, T., 2005. Long-chain alkenone distributions and temperature dependence in lacustrine surface sediments from China. Geochim. Cosmochim. Acta 69, 4985-5003.

Clark, P.U., Marshall, S. J., Garry, K.C. C., Hostetler, S.W., Licciardi, J.M., Teller, J.T., 2001, Freshwater Forcing of Abrupt Climate Change during the Last Glaciation. Science 293, 283-287.

Coolen, M.J.L., Muyzer, G., Rijpstra, W.I.C., Schouten, S., Volkman, J.K., Sinninghe Damsté, J.S., 2004. Combined DNA and lipid analyses of sediments reveal changes in Holocene haptophyte and diatom populations in an Antarctic lake. Earth Planet. Sci. Lett. 223, 225-239.

Cullen, H.M., deMenocal, P.B., Hemming, S., Hemming, G., Brown, F.H., Guilderson, T., Sirocko, F., 2000. Climate change and the collapse of the Akkadian empire: Evidence from the deep sea. Geology 28, 379-382.

Dean, W.E., 1974. Determination of carbonate and organic matter in calcareous sediments and sedimentary rocks by loss on ignition: comparison with other methods. Journal of Sedimentary Petrology, 44, 242-248.

D'Andrea, W.J., Huang, Y., Fritz, S.C., Anderson, N.J., 2011. Abrupt Holocene climate change as an important factor for human migration in West Greenland. Proc. Natl. Acad. Sci. USA 108, 9765-9769.

D'Andrea, W.J., Theroux, S., Bradley, R.S., Huang, X., 2016. Does phylogeny control UK37-temperature sensitivity? Implications for lacustrine alkenone paleothermometry. Geochim. Cosmochim. Acta 175, 168–180.

de Vernal, A., Hillaire-Marcel, C., Rochon, A., Fréchette, B., Henry, M., Solignac, S., Bonnet, S., 2013. Dinocyst-based reconstructions of sea ice cover concentration during the Holocene in the Arctic Ocean, the northern North Atlantic Ocean and its adjacent seas. Quat. Sci. Rev. 79, 111-121.

Dykoski, C.A., Edwards, R.L., Cheng, H., Yuan, D., Cai, Y., Zhang, M., Lin, Y., Qing, J., An, Z., Revenaugh, J., 2005. A high-resolution, absolute-dated Holocene and deglacial Asian monsoon record from Dongge Cave, China. Earth Planet. Sci. Lett. 233, 71-86.

Eldevik, T., Risebrobakken, B., Bjune, A. E., Andersson, C., Birks, H.J.B., Dokken, T.M., Drange, H., Glessmer, M.S., Li, C., Nilsen, J.E.Ø., Otterå, O.H., Richter, K., Skagseth, Ø., 2014. A brief history of climate – the northern seas from the Last Glacial Maximum to global warming: Quat. Sci. Rev. 106, 225-246.

Gao, L., Nie, J., Clemens, S., Liu, W., Sun, J., Zech, R., Huang, Y., 2012. The importance of solar insolation on the temperature variations for the past 110 kyr on the Chinese Loess Plateau. Palaeogeogr. Palaeoclimatol. Palaeoecol. 317–318, 128-133.

Goni, M.A., Woodworth, M.P., Aceves, H.L., Thunell, R.C., Tappa, E., Black, D., Müller-Karger, F., Astor, Y., Varela, R., 2004. Generation, transport, and preservation of the alkenone-based U37K′ sea surface temperature index in the water column and sediments of the Cariaco Basin (Venezuela). Global Biogeochem. Cycles 18, 1–21.

Grootes, P.M., Stuiver, M., White, J.W.C., Johnsen, S., Jouzel, J., 1993. Comparison of oxygen isotope records from the GISP2 and GRIP Greenland ice cores. Nature 366, 552-554.

Herzschuh, U., 2006. Palaeo-moisture evolution in monsoonal Central Asia during the last 50,000 years. Quat. Sci. Rev. 25, 163-178.

Hou, J., Huang, Y., Zhao, J., Liu, Z., Colman, S., An, Z., 2016. Large Holocene summer temperature oscillations and impact on the peopling of the northeastern Tibetan Plateau. Geophys. Res. Lett. 43, 1323-1330.

Jia, G., Rao, Z., Zhang, J., Li, Z., Chen, F., 2013. Tetraether biomarker records from a loess-paleosol sequence in the western Chinese Loess Plateau. Front. Microbiol. 4, 199.

Jin, L., Chen, F., Morrill, C., Otto-Bliesner B.L., Rosenbloom N., 2012. Causes of early Holocene desertification in arid central Asia. Clim. Dynam. 38, 1577-1591.

Kutzbach, J., Gutter, P., Behling, P.J. Selin, R., 1993. In Global Climates since the Last Glacial Maximum, eds Wright H. E, et al. (Univ. of Minnesota Press, MN), pp. 24–93.

Laskar, J., Robutel, P., Joutel, F., Gastineau, M., Correia, A.C.M., Levrard, B., 2004. A long term numerical solution for the insolation quantities of the Earth. Astron. Astrophys. 4, 261-285.

Linden, M., Möller, P.E.R., BjöRck, S., Sandgren, P.E.R., 2006. Holocene shore displacement and deglaciation chronology in Norrbotten, Sweden. Boreas 35, 1-22.

Liu, F., Feng, Z., 2012. A dramatic climatic transition at ~4000 cal. yr BP and its cultural responses in Chinese cultural domains. Holocene, 22, 1181-1197.

Liu, Z., Otto-Bliesner, B.L., He, F., Brady, E.C., Tomas, R., Clark, P.U., Carlson, A.E., Lynch-Stieglitz, J., Curry, W., Brook, E., Erickson, D., Jacob, R., Kutzbach, J., Cheng, J., 2009. Transient Simulation of Last Deglaciation with a New Mechanism for Bølling-Allerød Warming. Science 325, 310-314.

Liu, Z., Wen, X., Brady, E.C., Otto-Bliesner, B., Yu, G., Lu, H., Cheng, H., Wang, Y., Zheng, W., Ding, Y., Edwards, R. L., Cheng, J., Liu, W., Yang, H., 2014. Chinese cave records and the East Asia Summer Monsoon. Quat. Sci. Rev. 83, 115-128.

Longo, W.M., Dillon, J.T., Tarozo, R., Salacup, J.M., Huang, Y., 2013. Unprecedented separation of long chain alkenones from gas chromatography with a poly(trifluoropropylmethylsiloxane) stationary phase. Org. Geochem. 65, 94-102.

Longo, W.M., Theroux, S., Giblin, A.E., Zheng, Y.S., Dillon, J.T. Huang, Y., 2016. Temperature calibration and phylogenetically distinct distributions for freshwater alkenones: Evidence from northern Alaskan lakes. Geochim. Cosmochim. Acta 180, 177–196.

Ma Z., Wang Z., Liu J., Yuan B., Xiao J., Zhang G., 2004. U-series chronology of sediments associated with Late Quaternary fluctuations, Balikun Lake, northwestern China. Quatern. Int. 121, 89-98.

McManus, J.F., Francois, R., Gherardi, J.M., Keigwin, L.D., Brown-Leger, S., 2004. Collapse and rapid resumption of Atlantic meridional circulation linked to deglacial climate changes. Nature 428, 834-837.

Mercer, J.L., Zhao, M., Colman, S.M., 2005. Seasonal variations of alkenones and UK37 in the Chesapeake Bay water column. Estuar. Coast. Shelf S. 63, 675-682

Members, C., 1988. Climatic Changes of the Last 18,000 Years: Observations and Model Simulations. Science 241, 1043-1052.

Nakamura, H., Sawada, K., Araie, H., Suzuki, I., Shiraiwa, Y., 2014. Long chain alkenes, alkenones and alkenoates produced by the haptophyte alga Chrysotila lamellosa CCMP1307 isolated from a salt marsh. Org. Geochem. 66, 90-97.

Pearson, E.J., Juggins, S., Farrimond, P., 2008. Distribution and significance of long-chain alkenones as salinity and temperature indicators in Spanish saline lake sediments. Geochim. Cosmochim. Acta 72, 4035-4046.

Peterse, F., Prins, M.A., Beets, C.J., Troelstra, S.R., Zheng, H., Gu, Z., Schouten, S., Damsté, J.S.S., 2011. Decoupled warming and monsoon precipitation in East Asia over the last deglaciation. Earth Planet. Sci. Lett. 301, 256-264.

Porter, S.C., Zhisheng, A., 1995. Correlation between climate events in the North Atlantic and China during the last glaciation. Nature 375, 305-308.

Randlett, M.-È., Coolen, M.J.L., Stockhecke, M., Pickarski, N., Litt, T., Balkema, C., Kwiecien, O., Tomonaga, Y., Wehrli, B., Schubert, C.J., 2014. Alkenone distribution in Lake Van sediment over the last 270 ka: influence of temperature and haptophyte species composition. Quat. Sci. Rev. 104, 53-62.

Reimer, P.J., Bard, E., Bayliss, A., Beck, J.W., Blackwell, P.G., Bronk Ramsey, C., Buck, C.E., Cheng, H., Edwards, R.L., Friedrich, M., Grootes, P.M., Guilderson, T.P., Haflidason, H., Hajdas, I., Hatté, C., Heaton, T.J., Hoffmann, D.L., Hogg, A.G., Hughen, K.A., Kaiser, K.F., Kromer, B., Manning, S.W., Niu, M., Reimer, R.W., Richards, D.A., Scott, E.M., Southon, J.R., Staff, R.A., Turney, C.S.M., van der Plicht, J., 2013. IntCal13 and Marine13 Radiocarbon Age Calibration Curves 0–50,000 Years cal BP. Radiocarbon, 55, 1869–1887.

Renssen, H., Seppä, H., Heiri, O., Roche, D.M., Goosse, H., Fichefet, T., 2009. The spatial and temporal complexity of the Holocene thermal maximum. Nature Geoscience, 2, 411–414.

Renssen, H., Seppä, H., Crosta, X., Goosse, H., Roche, D.M., 2012, Global characterization of the Holocene Thermal Maximum. Quat. Sci. Rev. 48, 7-19.

Shakun, J.D., Clark, P.U., He, F., Marcott, S.A., Mix, A.C., Liu, Z., Otto-Bliesner, B., Schmittner, A., Bard, E., 2012. Global warming preceded by increasing carbon dioxide concentrations during the last deglaciation. Nature 484, 49-54.

Staubwasser, M., Sirocko, F., Grootes, P.M., Segl, M., 2003. Climate change at the 4.2 ka BP termination of the Indus valley civilization and Holocene south Asian monsoon variability. Geophys. Res. Lett., 30, 1425.

Sun, Q., Chu, G., Liu, G., Li, S., Wang, X., 2007. Calibration of alkenone unsaturation index with growth temperature for a lacustrine species, Chrysotila lamellosa (Haptophyceae). Org. Geochem. 38, 1226-1234.

Theroux, S., D'Andrea, W.J., Toney, J., Amaral-Zettler, L., Huang, Y., 2010, Phylogenetic diversity and evolutionary relatedness of alkenone-producing haptophyte algae in lakes: Implications for continental paleotemperature reconstructions. Earth Planet. Sci. Lett. 300, 311-320.

Theroux, S., 2012. Diversity and Ecology of Lacustrine Haptophyte Algae: Implications for Paleothermometry. PhD Thesis, Brown University.

Theroux, S., Toney, J., Amaral-Zettler, L., Huang, Y., 2013. Production and temperature sensitivity of long chain alkenones in the cultured haptophyte Pseudoisochrysis paradoxa. Org. Geochem. 62, 68-73.

Toney, J.L., Huang, Y., Fritz, S.C., Baker, P.A., Grimm, E., Nyren, P., 2010. Climatic and environmental controls on the occurrence and distributions of long chain alkenones in lakes of the interior United States. Geochim. Cosmochim. Acta 74, 1563-1578.

Toney, J.L., Theroux, S., Andersen, R.A., Coleman, A., Amaral-Zettler, L., Huang, Y., 2012. Culturing of the first 37:4 predominant lacustrine haptophyte: Geochemical, biochemical, and genetic implications. Geochim. Cosmochim. Acta 78, 51-64.

Wang, S.M., Dou, H.S., 1998. Chinese Lakes Memoir. Science Press, Beijing, p. 354 (in Chinese).

Wang, Y., Cheng, H., Edwards, R.L., Kong, X., Shao, X., Chen, S., Wu, J., Jiang, X., Wang, X., An, Z., 2008. Millennial- and orbital-scale changes in the East Asian monsoon over the past 224,000 years. Nature 451, 1090-1093.

Wang, Z., Liu W., 2013. Calibration of the UK’37 index of long-chain alkenones with the in-situ water temperature in Lake Qinghai in the Tibetan Plateau. Chin. Sci. Bull. 58, 803-808.

Wang, Z., Liu, Z., Zhang, F., Fu, M., An, Z., 2015. A new approach for reconstructing Holocene temperatures from a multi-species long chain alkenone record from Lake Qinghai on the northeastern Tibetan Plateau. Org. Geochem. 88, 50-58.

Weiss, H., Bradley, R.S., 2001. What Drives Societal Collapse? Science 291, 609-610.

Weiss, H., Courty, M. A., Wetterstrom, W., Guichard, F., Senior, L., Meadow, R., Curnow, A., 1993. The Genesis and Collapse of Third Millennium North Mesopotamian Civilization. Science 261, 995-1004.

Wen, R., Xiao, J., Chang, Z., Zhai, D., Xu, Q., Li, Y., Itoh, S., 2010. Holocene precipitation and temperature variations in the East Asian monsoonal margin from pollen data from Hulun Lake in northeastern Inner Mongolia, China. Boreas 39, 262-272.

Wu, W., Liu, T., 2004. Possible role of the “Holocene Event 3” on the collapse of Neolithic Cultures around the Central Plain of China. Quat. Int., 117, 153-166.

Xiao, J., Xu, Q., Nakamura, T., Yang, X., Liang, W., Inouchi, Y., 2004. Holocene vegetation variation in the Daihai Lake region of north-central China: a direct indication of the Asian monsoon climatic history. Quat. Sci. Rev. 23, 1669-1679.

Xue, J., Zhong, W., 2011. Holocene climate variation denoted by Barkol Lake sediments in northeastern Xinjiang and its possible linkage to the high and low latitude climates. Sci. China Earth Sci. 54, 603-614.

Zhao, J., An, C., Longo, W.M., Dillon, J.T., Zhao, Y., Shi, C., Chen, Y., Huang, Y., 2014. Occurrence of extended chain length C41 and C42 alkenones in hypersaline lakes. Org. Geochem. 75, 48-53.

Zhao J., Lai, Z., Liu, S., Song, Y., Li, Z., Yin, X., 2012. OSL and ESR dating of glacial deposits and its implications for glacial landform evolution in the Bogeda Peak area, Tianshan range, China. Quat. Geochronol. 10, 237-243.

Zhao, Y., An, C.-B., Mao, L., Zhao, J., Tang, L., Zhou, A., Li, H., Dong, W., Duan, F., Chen, F., 2015. Vegetation and climate history in arid western China during MIS2: New insights from pollen and grain-size data of the Balikun Lake, eastern Tien Shan. Quat. Sci. Rev. 126, 112-125.

Zheng, X.Y., et al., 1995, Salt lake in Xinjiang: Beijing, Science press (in Chinese).

Zheng, Y.S., Huang, Y., Andersen, R.A., Amzral-Zettler, L.A., 2016. Excluding the di-unsaturated alkenone in the UK37 index strengthens temperature correlation for the common lacustrine and brackish-water haptophytes. Geochim. Cosmochim. Acta 175, 36-46.

Zhou, T., Gong, D., Li, J., Li, B., 2009. Detecting and understanding the multi-decadal variability of the East Asian Summer Monsoon recent progress and state of affairs. Meteorol.Z. 18, 455-467.

Zhu, C., Chen, X., Zhang, G., Ma, C., Zhu, Q., Li, Z., Xu, W., 2008. Spore-pollen-climate factor transfer function and paleoenvironment reconstruction in Dajiuhu, Shennongjia, Central China. Chin. Sci. Bull. 53, 42-49.

Table

Table 1 AMS radiocarbon dates and dated material from core BLK11A in Lake Balikun.

Figure Captions

Figure 1. Summer (June-July-August, JJA) mean 700 hPa streamline based on NCEP/NCAR Reanalysis during 1971–2000. Red star indicates the location of Lake Balikun. 'EASM', 'ISM', and 'Westerlies' denote the regions mainly influenced by the East Asian Summer Monsoon, the Indian Summer Monsoon, and the Westerlies, respectively. Triangles indicate the caves mentioned in the text, Dongge cave (25°17′ N, 108°5′ E) and Hulu cave (32°30′ N, 119°10′ E). Blue dots indicate the lakes mentioned in the text, Lake Qinghai (36°32′-37°15′ N, 99°36′-100°47′ E); Lake Gonghai (38°54′ N, 112°14′ E); Lake Daihai (40°29′-40°37′ N, 112°33′-112°46′ E); Lake Hulun (49°7.6′ N, 117°30.4′ E). Blue square indicates ice cores (49°48′ N, 86°33′ E) from the Altai Mountains

Figure 2. Chronology and lithology of sediment cores (BLK11A) from Lake Balikun

Figure 3. U_{37}^{k} and $U_{37}^{k\prime}$ vs. *in-situ* water temperature in water filter samples. The three open circles are excluded from calibration equation, since these samples were collected from near shore locations. Alkenones in these samples may not have been produced in situ because of highly dynamic nature of the near shore lake waters.

Figure 4. Organic geochemical and other environmental proxies past 21 kyr from Lake Balikun. (a) LCAs concentrations; (b) LOI (550 °C); (c) carbonate content. The percentage of Artemisia (d) and Betula (e) pollen and vegetation types from BLK06E core (An et al., 2012, 2013).

Figure 5 Alkenone signatures: Surface water filter sample (a) and Type I alkenone profile (b) from BLK11A core at 266 cm.

Figure 6 Type II alkenone profile (a: from BLK11A core at 600 cm), *P. Paradoxa* alkenone profile (b: Theroux et al., 2013) and *C. lamellosa* alkenone profile (c: Sun et al., 2007).

Figure 7. Principal component analysis (PCA) of LCAs index used in this study. Specifically, in order to best differentiate the two haptophyte species, we use a number of

ratios derived from C_{37} and C_{38} alkenones as variables for principal component analysis (PCA). These ratios include: $\%C_{37:4}$ / $\%C_{38:4}$, $\%C_{37:4}$ / $\%C_{38:3}$, $\%C_{37:4}$ / $\%C_{38:2}$, $\%C_{37:3}$ / $\%C_{38:4}$, $\%C_{37:3}$ / $\%C_{38:3}$, $\%C_{37:3}$ / $\%C_{38:2}$, $\%C_{37:2}$ / $\%C_{38:4}$, $\%C_{37:2}$ / $\%C_{38:3}$, $\%C_{37:2}$ / $\%C_{38:2}$ and C_{37} / $C_{38.}$ Note $\%C_{37:4}$ represents percentage of $C_{37:4}$ alkenone relative to all C_{37} alkenones (i.e., percentage ratio of $C_{37:4}$ over the sum of $C_{37:2}$ + $C_{37:3}$ + $C_{37:4}$). Same is true for $\%C_{38:4}$, $\%C_{38:3}$ etc. The red circles indicate type I, and the blue circles indicate type II. The green circles indicate water filter samples.

Figure 8. Comparison of Lake Balikun records with model results. (a) Alkenone-based June-July temperature in Lake Balikun; (b) $\%C_{37:4}$; (c) Percentage of Artemisia pollen in Lake Balikun (An et al., 2012b, 2013). Surface temperature (d) and annual precipitation (e) time series from the CCSM3 TraCE transient simulation was produced from the grid cell near the Lake Balikun (40 °N, 93 °E) (Liu et al., 2009). Yellow shadows indicate the difference between Lake Balikun records and model results.

Figure 9. Comparison of Lake Balikun records with other records. (a) Alkenone-based June-July temperature in Lake Balikun and June-July insolation at 43 °N (Laskar et al., 2004); (b) Percentage of Artemisia pollen in Lake Balikun (An et al., 2012, 2013); (c) Temperature record from Lake Qinghai (Hou et al., 2016); (d) Lake Qinghai Asian summer monsoon index (SMI) (Z. An et al., 2012); (e) Pollen-based annual precipitation reconstructed from Gonghai Lake (Chen et al., 2015); (f) Dongge and Hulu cave speleothem $\delta^{18}O$ records, respectively (Dykoski et al., 2005; Wang et al., 2008); (g) Reconstructed sea ice extent at Barents Sea (de Vernal et al., 2013); (h) Reconstructed strength of Norwegian Atlantic Current (Eldevik et al., 2014); (i) Western subtropical Atlantic $^{231}Pa/^{230}Th$ record (red and green circles denote measurements using two different methods; error bars: 2σ), and synthesized meltwater flux in the Northern Hemisphere (blue line) (McManus et al., 2004; Liu et al., 2014); (j) The Greenland Ice Sheet Project 2 (GISP2) $\delta^{18}O$ record (Grootes et al., 1993).

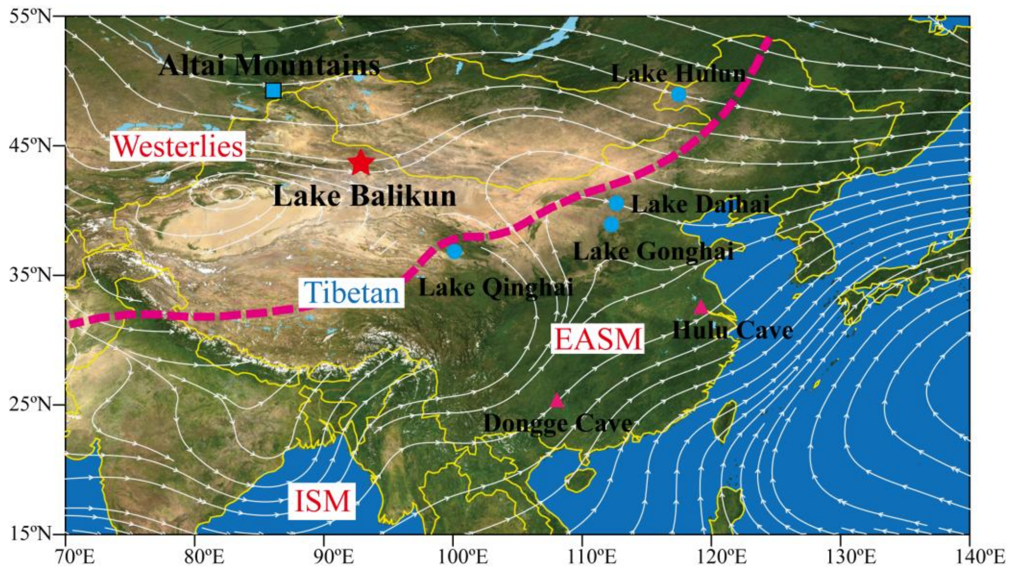
55ºN
45ºN
35ºN
25ºN
15ºN
70ºE
80ºE
90ºE
100ºE
110ºE
120ºE
130ºE
140ºE
Altai Mountains
Lake Hulun
Westerlies
Lake Balikun
Lake Daihai
Lake Gonghai
Tibetan
Lake Qinghai
Hulu Cave
EASM
Dongge Cave
ISM

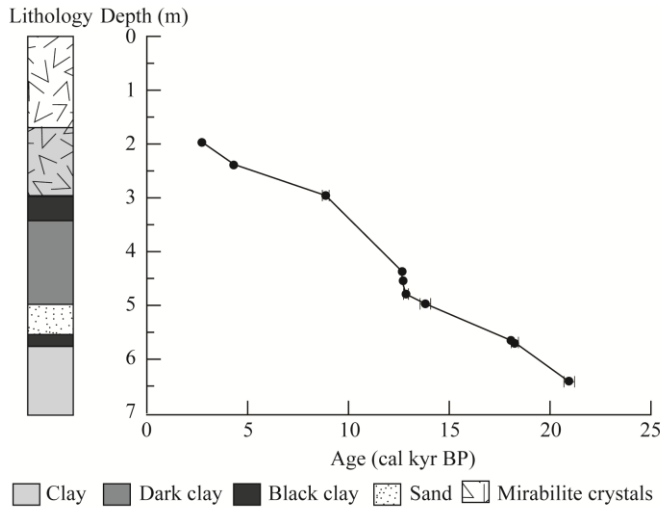
Lithology
Depth (m)
0
1
2
3
4
5
6
7
0
5
10
15
20
25
Age (cal kyr BP)
Clay
Dark clay
Black clay
Sand
Mirabilite crystals

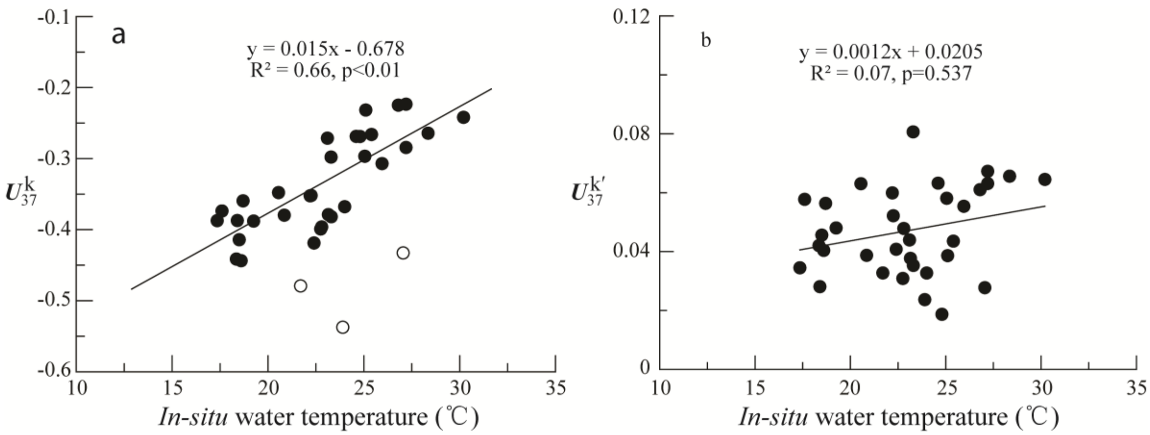
a
y = 0.015x - 0.678
R² = 0.66, p<0.01
U_{37}^{k}
-0.1
-0.2
-0.3
-0.4
-0.5
-0.6
10
15
20
25
30
35
In-situ water temperature (℃)
b
y = 0.0012x + 0.0205
R² = 0.07, p=0.537
$U_{37}^{k'}$
0.12
0.08
0.04
0
10
15
20
25
30
35
In-situ water temperature (℃)

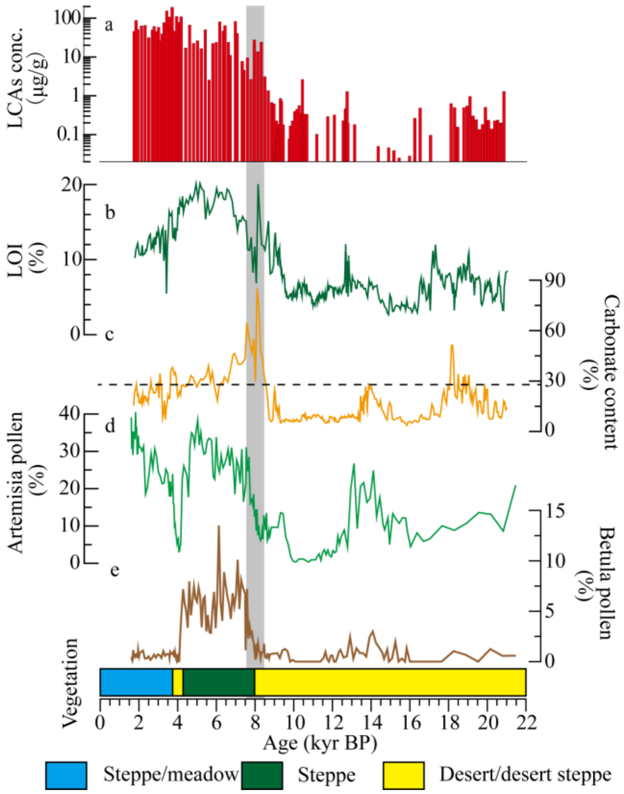

LCAs conc. (μg/g)
100
10
1
0.1
a
LOI (%)
20
10
0
b
c
Carbonate content (%)
90
60
30
0
Artemisia pollen (%)
40
30
20
10
0
d
e
Betula pollen (%)
15
10
5
0
Vegetation
0 2 4 6 8 10 12 14 16 18 20 22
Age (kyr BP)
Steppe/meadow
Steppe
Desert/desert steppe

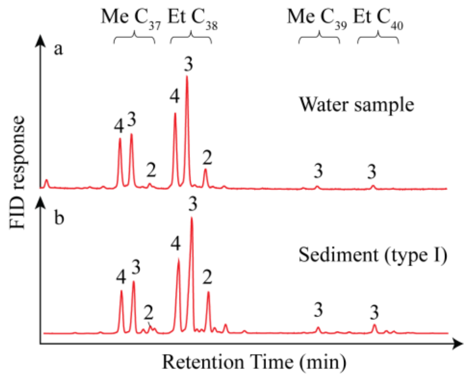
Me C_{37} Et C_{38}
Me C_{39} Et C_{40}
a
Water sample
b
Sediment (type I)
FID response
Retention Time (min)

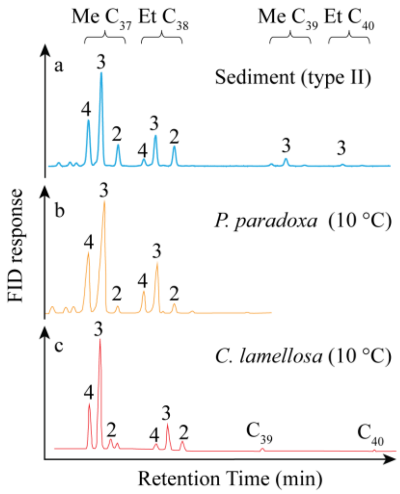
Me C37 Et C38
Me C39 Et C40
a
Sediment (type II)
b
P. paradoxa (10 °C)
c
C. lamellosa (10 °C)
C39
C40
FID response
Retention Time (min)

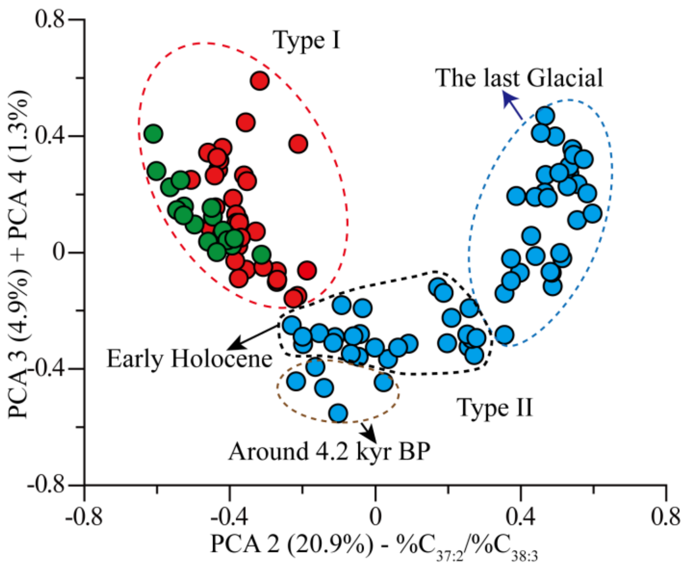

Type I
The last Glacial
Early Holocene
Type II
Around 4.2 kyr BP
PCA 3 (4.9%) + PCA 4 (1.3%)
PCA 2 (20.9%) - %C37:2/%C38:3
0.8
0.4
0
-0.4
-0.8
-0.8
-0.4
0
0.4
0.8

700

701

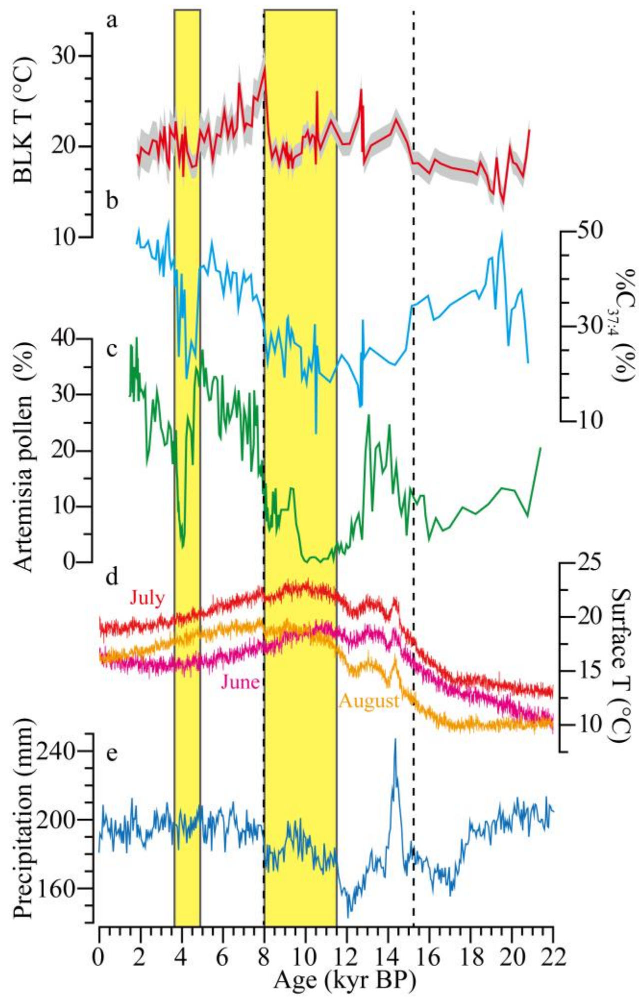

a
b
c
d
e
BLK T (°C)
%C37:4 (%)
Artemisia pollen (%)
Surface T (°C)
Precipitation (mm)
July
June
August
Age (kyr BP)

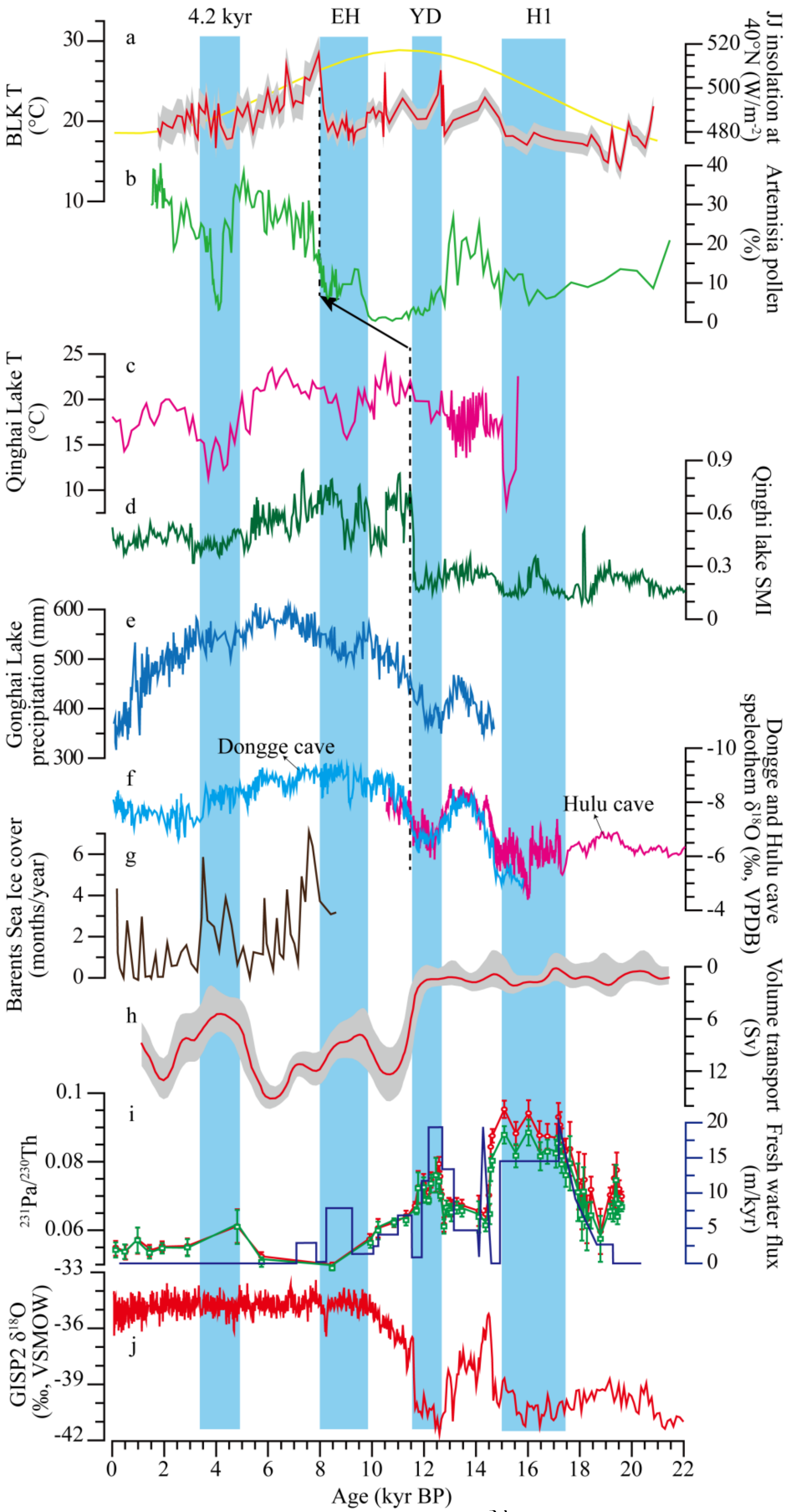

4.2 kyr
EH
YD
H1
a
b
c
d
e
f
g
h
i
j
BLK T (°C)
JJ insolation at 40°N (W/m-2)
Artemisia pollen (%)
Qinghai Lake T (°C)
Qinghi lake SMI
Gonghai Lake precipitation (mm)
Dongge cave
Hulu cave
Dongge and Hulu cave speleothem δ18O (‰, VPDB)
Barents Sea Ice cover (months/year)
Volume transport (Sv)
231Pa/230Th
Fresh water flux (m/kyr)
GISP2 δ18O (‰, VSMOW)
Age (kyr BP)

Table 1 AMS radiocarbon dates and dated material from core BLK11A in Lake Balikun.

Lab code	**Depth (cm)**	**Material Dated**	**$\delta^{13}C$ (‰)**	**Conventional radiocarbon age (yr BP)**	**Reservoir-corrected ^{14}C age by 790 yr**	**2-sigma calibrated age range (cal. yr BP)**
345869	197	Bulk clay	-23.5	3420±30	2630±30	2728-2786
345870	238	Bulk clay	-20.6	4690±30	3900±30	4247-4418
345871[a]	293	Bulk clay	-19.3	8860±40	8070±40	8779-9093
345873[a]	437	Charcoal	-11.6	11520±50	10730±50	12587-12732
376479[a]	453	Charcoal	-11.3	11480±40	10690±40	12576-12715
377642[a]	479	Charred seeds	-16.7	11770±40	10980±40	12727-12974
345874[a]	497	Bulk clay	-22.9	12750±50	11960±50	13619-14003
345875[a]	565	Bulk clay	-21	15630±60	14840±60	17867-18246
377643[a]	569	Charred seeds	-10.1	15820±60	15030±60	18045-18452
345881[a]	642	Plant macrofossils	-11.8	18150±70	17360±70	20695-21202

[a] data from Zhao et al., 2015